INVESTIGATIONS INTO THE FLOW BEHIND CASTELLATED BLUNT TRAILING EDGE AEROFOILS IN SUPERSONIC FLOW

S. L. Gai, E. C. Magi and A. Prytz

Department of Mechanical Eng'g, University College, UNSW,
Australian Defence Force Academy, Campbell, A.C.T. 2600, Australia.

Abstract

The paper reports an investigation into the flow behind the base of a castellated blunt trailing edge aerofoil at supersonic speeds at a Mach number of 2. The investigation has shown that strong gradients exist in the spanwise direction and the formation of the wake shock occurs further away from the wake axis and the wake neck is broader and diffused. This would indicate that the vortex street that is formed at the base of the shock becomes weaker. A theoretical analysis based on vorticity conservation would then suggest that part of the spanwise vorticity must be transformed into streamwise vorticity and hence result in decreased drag. Detailed data involving pressure measurements, Schlieren and holographic interferometry and Laser velocimetry are presented.

Introduction

Although a blunt trailing edge has advantages at transonic and supersonic speeds, it creates high base drag at subsonic speeds due to periodic vortex shedding. Techniques such as splitter plates and base bleed have been used in the past to alleviate this problem.[1,2] A relatively new technique, that of castellating a blunt trailing edge, thus providing a discontinuous separation line, has been shown to be quite effective in recent years.[3,4,5]

However, very little is known about the behaviour of a castellated blunt trailing edge aerofoil at supersonic speeds although some preliminary (unpublished) work at the University of Bristol in the early seventies suggested that some base drag reductions are achievable. The mechanism of this base pressure recovery, though, is not yet fully understood. The subject has particular relevance with respect to the design of supersonic/hypersonic aircraft and missiles and wake flows behind cascades of turbine blades.

A study of the near wake flow of castellated trailing edge aerofoils at Mach 2 was therefore undertaken to increase the available data base and to understand the mechanism of base pressure recovery. This paper presents some of the results obtained during the course of this study.

Experimental Arrangement

The experiments were carried out in a blow down supersonic wind tunnel of cross section 155 mm x 90 mm at a Mach number $M_\infty \approx 2.0$ and a Reynolds number based on chord length in the range $2 \times 10^6 \lesssim Re_c \lesssim 9 \times 10^6$.

The models had a wedge shaped leading edge followed by a flat plate with a blunt trailing edge. The base height 'h' for all the models was 6 mm. In order to study both streamwise and transverse flow (across span) behind the base two series of models were constructed. Those constructed to look at the streamwise flow were horizontally mounted and had a chord length of 130 mm. Those constructed to study transverse features of the flow had a chord of 75 mm.

The details of the castellated blunt trailing edge models were as follows:
(a) for horizontally mounted models the spacing ratios were bxa = 18 mm x 6 mm; 18 mm x 12 mm; 18 mm x 18 mm;12 mm x 6 mm; and 12 mm x 12 mm.
(b) for vertically mounted models
bxa = 18 mm x 6 mm; 18 mm x 12 mm; 18 mm x 18 mm; 12 mm x 6 mm; 12 mm x 12 mm; and 12 mm x 18 mm.

The nomenclature is indicated in Fig.1(a) and the photograph of a typical model is shown in Fig.1(b).
It will be seen that for both series of models the aspect ratio AR (b/a) of the castellations varied from 2/3 to 3.
To compare the results of a blunt castellated trailing edge, experiments were also conducted with a plain blunt trailing edge. This had a base height of 6 mm, chord length of 130 mm and was horizontally mounted.

The techniques employed for acquisition of data consisted of base pressure measurements, pitot traverses in the near wake, Schlieren and shadowgraph photography, holographic interferometry and Laser two focus (L2F) velocimetry. Taken together, they have provided an understanding of the flow mechanism behind a castellated blunt trailing edge aerofoil at supersonic speeds.

Results and Discussion

The Plain Blunt Trailing Edge

The supersonic base flow of a two-dimensional blunt base can be conveniently divided into various flow regimes. The separating flow undergoes an expansion around the corner, forming a recirculation region behind the base. A free shear layer separates the recirculation region from the expansion fan. The flow recompresses approximately one to three base heights downstream of the base forming a wake neck and a wake shock which then turns the flow back to the free stream direction. The expansion fan is sometimes terminated by a lip shock (Fig.2). The lip shock recompresses the over expanded flow to the base pressure. Hama[6] has shown that the location and strength of the lip shock depends on the Reynolds number, Mach number and the base geometry.

It has been known that for a given Mach number and geometry, the base pressure is a

function of the Reynolds number Re_c. Figure 3 shows the results obtained in this investigation. The variation in Reynolds number was achieved by varying the stagnation pressure. These results suggest that transition region lies in the range $3x10^6 \lesssim Re_c \lesssim 7x10^6$. For Reynolds numbers above $7x10^6$ the base pressure appears to correlate well with Chapman's[7] correlating parameter for turbulent flow.

The Castellated Trailing Edge

The study of the flow behind a castellated trailing edge was done in four parts. First the base pressure measurements; second, Schlieren and shadowgraph photography and holographic interferometry viewing along and on to the span; third, pitot traverses in the wake; and finally Laser 2 Focus velocimetry.

Considering base pressure measurements, Fig.4 shows the base pressures obtained on the projections and recesses. The striking feature is the existence of large spanwise gradients. Further, it is seen that the mean base pressure coefficient of a castellated trailing edge is higher than that of the plain blunt trailing edge, thus yielding a reduction in the base drag. For the trailing edge geometry shown in Fig.4 this is of the order of 15 per cent. Results of base pressure measurements for other geometries showed similar spanwise variation.

The amount of base pressure recovery, however, seemed to depend on the aspect ratio of the castellations. This is shown in Fig.5. 1/AR=0 corresponds to the plain base. It is seen that recovery is less for larger aspect ratio models and for AR > 2, the mean base pressure coefficient is approximately the same as for the plain base. From the results the optimum aspect ratio appears to lie between 1 and 2/3. Also shown on this figure are the results of Steen[8] which are the only ones available for comparison. They too indicate a similar trend.

From Fig.4 we also see that across individual projections and recesses large pressure gradients exist with higher pressure regions in the centres. Figure 6 shows some results obtained on projection elements. We note that large spanwise gradients exist with high pressures at the centre and low pressures at the recess/projection boundary. These gradients are quite strong for AR > 1. We also note that with the decrease in the aspect ratio, the gradients are significantly decreased and at the same time the mean base pressure is increased. When AR<1 the pressure distribution is almost flat and the base pressure is maximum. It is also interesting to note that the pressure distributions are remarkably symmetrical.

The recess pressure distributions behaved in a similar way in that the mean base pressure of the recess also increased with the decrease in the aspect ratio. However, there seemed to be some dependence on the projection width in that the gradients across the recess span were considerably larger for a smaller projection width (b/h = 2) than for the larger one with b/h = 3.

Taken together, measurements on individual castellation elements reinforce the inference of Fig.5.

The next step was to supplement the base pressure data with flow visualisation. Figures 7(a) through (e) show some of the photographs obtained.

Figure 7(a) shows a typical shadowgraph of the flow behind a castellated trailing edge model. We notice that the wake neck is significantly thicker than that of the plain blunt trailing edge. The wake shock appears to form further away from the axis and its origin is approximately two base heights downstream of the trailing edge.

Referring to Fig.7(b), the differential holographic interferogram of the flow behind a castellated trailing edge, we can see that the wake shock behind the recess attenuates to a Mach wave at about 8 to 10 base heights downstream. The interferogram clearly shows the nature of the unsteady turbulent wake behind the neck and that the neck is wide and not as clearly defined as in the case of the plain blunt trailing edge.

Viewing along the span of the model, the Schlieren photograph shown in Fig.7(c) indicates a highly three dimensional wake with strong gradients in the spanwise direction. In particular, shear layers springing from projections and recesses are contracting and expanding respectively. The flow forms a pattern similar to a series of over and under expanded jets. The spanwise gradients persist several base heights downstream and are located in cells formed by expansion and compression waves. Figures 7(d) and (e) show similar features but with different aspect ratio constellations. It is clear from comparison of photographs 7(c),(d) and (e) that spanwise gradients become stronger with decrease in aspect ratio, which again is consistent with the composite result shown in Fig.5.

The flow visualisation results thus confirm the existence of a spanwise gradient as a result of entrainment of the flow from the top of the projection into the recess which is then recompressed and thereafter expands round the projection tips. The pressure distribution on the projection is also characterised by a large transverse gradient with the lowest pressures at the tips. This gradient is a result of the fluid entrained from the top of the projection elements into the recesses as described above. A pressure mismatch therefore occurs between the out flow from the recess and the corner of the projection and the flow from the recess expands around the projection tips and the wake is characterised by a series of expansion and compression waves.

Figure 8 shows some results of pitot pressure traverses made in the wake of a castellated blunt trailing edge aerofoil. These traverses were made behind the centre line of the projection, the recess, and along the recess/projection edge. For comparison, plain blunt base results are also shown. The figure shows the strength of the recompression shock

expressed in terms of the ratio of measured pitot pressure across the shock.

An interesting feature is that the recess shock is weaker than that of the projection while the fully formed wake shock of the plain base is stronger than either of the two. These results are consistent with the flow photographs of Fig.2 and 7(a). It is also important to note that the shock strength at the recess/projection edge is weakest which is consistent with the fact that there is strong expansion around the tips as described earlier.

Laser Two Focus (L2F) Velocimetry Data

The L2F system used was a Polytec system with a 2.5 W argon-ion laser and a signal processor. The beam diameter at the focal plane was 10 μm and the beam separation was 225 μm. The theory of operation of the L2F system has been described elsewhere.[9] Briefly, the measuring direction is in a plane containing the focal volumes as shown in Fig.9. The light scattered by particles passing through the two focii is sensed by two photomultipliers, one for each focus. The signal from each focus is amplified and the time of flight of a particle is then measured by a time-to-pulse-height converter (TPHC) which generates an output pulse proportional to the time interval between a start and stop pulse. The output of the TPHC is then digitised by a multichannel analyser which produces a histogram of times of flight, from which velocity distribution may be derived. The details of extracting turbulence data from the basic measurement is described by Prytz.[9] In the present set up, the beam was traversed across the wake by placing the Laser system on a milling machine platform and traverses were possible in all the three co-ordinate directions.

Figures 10(a),(b) and (c) show the velocity contour map behind a plain blunt trailing edge and behind the centre line of the projection and recess of a castellated trailing edge. Considering the castellated trailing edge first, we note that behind the projection the wake neck is quite well defined while the flow behind the recess is diffused with smaller velocity fluctuations. The flow behind the plain blunt trailing edge is similar to that behind the projection.

Figures 11(a),(b) and (c) show the longitudinal turbulent intensity behind the plain blunt trailing edge and the castellated blunt trailing edge. Firstly we note that levels of turbulent intensity behind the recess are quite low compared to that of projection. Secondly the turbulent intensities behind the projection are comparable to that of the plain blunt trailing edge but fluctuations behind the plain blunt trailing edge seem more severe. The lateral turbulent intensity measurements $\langle v' \rangle$ showed similar results.

Thus the velocity and turbulence measurements show the diffused nature of the flow behind the recess and the existence of spanwise gradients in the flow consistent with pressure and flow visualisation data.

A MECHANISM FOR DRAG REDUCTION

The drag reduction in subsonic flow is primarily due to the perturbation and break up of two dimensional vortex shedding.[10,11] The amount of fluid being entrained and convected away from the base by the vortices depends on the strength and orientation of the vorticity axis. With the discontinuous trailing edge of a castellated base, the separating vortex filaments associated with the boundary layer are skewed and there is a strong streamwise component of the vorticity.[12]

At supersonic Mach numbers, the mixing layers are stable and the vortex street that is formed at the base of the trailing shock is very weak and eventually decays downstream of the neck with vortex like structures (Fig. 7(b)) which are essentially random. Thus one can consider that most of the vorticity is concentrated in the neck region.[13]

Since it is the vorticity being generated in the boundary layers upstream that is convected into the wake, we can trace the vorticity content as it travels down the wake and the circulation associated with it. This approach is based on the 'vorticity tube' concept proposed by Liang & Bershader.[14]

The concept of the vorticity tube arises from the fact that vorticity Ω and the mass flux (ρu) are governed by similar transport equations. If we assume inviscid flow and a streamwise pressure gradient, the equations are

$$\frac{D\Omega}{Dt} + \Omega \operatorname{div} \tilde{u} - \frac{1}{\rho^2}\frac{\partial \rho}{\partial y}\frac{dP}{dx} = 0$$

and (1)

$$\frac{D(\rho u)}{Dt} + (\rho u) \operatorname{div} \tilde{u} + \frac{dP}{dx} = 0$$

The vorticity tube $\Omega A^* = \text{const.}$ is analogous to a stream tube $\rho u A = \text{const.}$ where A^* and A are areas of cross section of the vorticity and stream tubes respectively. The boundary of the vorticity tube is where $\Omega = 0$. Thus the shear layer or wake edge and lines of symmetry of velocity profiles such as wake axis can be thought of as 'walls' of vorticity tube. On the other hand, solid boundaries represent a source or sink of vorticity.

The vorticity Ω has the circulation Γ associated with it so that

$$\Omega = \frac{d\Gamma}{dA^*} = \frac{d\Gamma}{dt}\frac{dt}{dA^*} \qquad (2)$$

This can be rearranged to be

$$\Omega \frac{dA^*}{dt} = \frac{d\Gamma}{dt} \qquad (3)$$

The rate of change in circulation is equal to the specific work done on the fluid element so that

$$\frac{d\Gamma}{dt} = -\int_{path} Tds = -T_\infty \delta s \qquad (4)$$

Now, the equation of the vorticity tube can be rewritten in differential form such that

$$\frac{d(\Omega A^*)}{dt} = 0 = \frac{\Omega dA^*}{dt} + \frac{A^* d\Omega}{dt} \qquad (5)$$

giving

$$\frac{\Omega dA^*}{dt} = \frac{-A^* d\Omega}{dt} = -T_\infty \delta s \qquad (6)$$

from which

$$A^* \frac{d\Omega}{dt} = T_\infty \delta s \qquad (7)$$

Now, this can be expressed as

$$\frac{d}{dt}\left(A^* \frac{d\Omega}{dt}\right) = T_\infty \frac{ds}{dt} \qquad (8)$$

or

$$\frac{d}{dt}\left(A^* \frac{d\Omega}{dt}\right) = \frac{T_\infty}{m} \frac{dS}{dt} \quad (\because S = ms)$$

Then, expanding the L.H.S. of the equation,

$$\frac{dA^*}{dt}\frac{d\Omega}{dt} + A^* \frac{d^2\Omega}{dt^2} = \frac{T_\infty}{m}\frac{dS}{dt} \qquad (9)$$

For a flow which is steady in the mean the second term on the L.H.S. vanishes, so that

$$\frac{dA^*}{dt}\frac{d\Omega}{dt} = \frac{T_\infty}{m}\frac{dS}{dt} \qquad (10)$$

From Oswatitisch's theorem, relating drag and entropy,

$$DU_\infty = T_\infty \frac{dS}{dt} \qquad (11)$$

so that eqn.(10) becomes

$$m\frac{dA^*}{dt}\frac{d\Omega}{dt} = DU_\infty \qquad (12)$$

Now,

$$\frac{dA^*}{dt} = \frac{dA^*}{dx}\frac{dx}{dt} = U_e \frac{dA^*}{dx}$$

where U_e is the velocity at the edge of the vorticity tube (wake).
Then eqn.(12) can be written as

$$mU_e \frac{dA^*}{dx}\frac{d\Omega}{dt} = DU$$

or

$$D = m\left(\frac{U_e}{U_\infty}\right)\left(\frac{dA^*}{dx}\frac{d\Omega}{dt}\right) \qquad (13)$$

To a first approximation, from the neck downstream, $U_e \approx U_\infty$ so that

$$D \sim \left[\frac{dA^*}{dx}\frac{d\Omega}{dt}\right] \qquad (14)$$

From this relation we can see that drag is related to the rate of change in vorticity and the change in area of the vorticity tube. Now, it is well known[15] that the vorticity of a fluid particle can vary with time in two ways: firstly, when there exists a velocity gradient that is not normal to the existing vorticity axis; secondly, when there are accelerations/decelerations in the flow.

If, in the light of this, we examine the results of a castellated trailing edge, we find that the effect of castellations is to introduce strong transverse gradients in the velocity and accelerating and decelerating flows across recesses and projections so that $(\frac{d\Omega}{dt})$ should decrease. Also, for the drag to decrease 'the vorticity tube' cross section should increase. Experiments show that this is in fact the case. Compared to the neck of a plain blunt trailing edge, where essentially the vorticity is concentrated, the neck and subsequent wake of a castellated trailing edge is wider and diffuse. Hence, by Eqn.(14), drag of a castellated trailing edge should be smaller compared to that of a plain blunt trailing edge. Further, if globally the vorticity axis is spanwise, then the effect of transverse gradients is to skew the vortex filaments, thus producing streamwise vorticity. Features consistent with streamwise vortex cores have been observed in Schlieren photographs sensitive to spanwise density gradients. (Fig.7(c)). The above analysis thus qualitatively explains the mechanism of drag reduction from a castellated blunt trailing edge aerofoil.

CONCLUSIONS

Comparison of results between the plain blunt trailing edge aerofoil and castellated blunt trailing edge aerofoil has shown that considerable base pressure recovery occurs with a castellated blunt trailing edge. This, together with the fact that castellated blunt trailing edge aerofoils have advantages in subsonic and transonic flows means that they should be given serious consideration in the design of supersonic wings and control surfaces as well as turbine blades.

The drag reduction due to castellated blunt trailing edge seems primarily due to the segmentation of the flow and the resulting spanwise gradients that are set up. Based on pressure, flow visualisation and velocity data, a mechanism for this drag reduction has been suggested. It has also been shown that the base pressure recovery is a very strong function of the aspect ratio of the castellation. From the present data it appears that the optimum value of this aspect ratio for maximum pressure recovery lies between 1 and 2/3.

A qualitative theoretical explanation for the reduction of base drag has been proposed which is consistent with the experimental data.

Acknowledgements

Grateful acknowledgements are due to the Australian Research Grants Scheme for supporting Mr A. Prytz during the course of this work.

REFERENCES

1. Bearman, P.W., J. Fluid Mech., Vol. 21, p.241, 1965.
2. Bearman, P.W., The Aero. Quart., Vol. 18, p.207, 1967.
3. Tanner, M., The Aero. Quart., Vol. 23, p.15, 1972.
4. Pollock, N., ARL (Australia), Rept. No. 137, 1972.
5. Gai, S.L. & Sharma, S.D., Aeronautical J., The Roy. Aero. Soc., Vol. 85, p. 206, 1981.

6. Hama, F.R., AIAA J., Vol. 6, p.212, 1968.
7. Chapman, D.R., NACA Rept. No. 1051, 1951.
8. Steen, P.H., B.Sc. Thesis, Aero. Engg. Dept., Univ. of Bristol, June 1975 (unpublished).
9. Prytz, A., 'A2F' Polytec L2F Hardware Program Rept., Dept. of Mech. Engg. ADFA, 1989.
10. Naumann, A., Morsbach, M. & Kramer, C., AGARD Conf. Proc. No.4, Pt.2, p.539, 1966.
11. Gai, S.L. & Sharma, S.D., Paper No. 13C, Proc. 8th Australasian Fluid Mech. Conf., Newcastle, Australia, 1983.
12. Petrusma, M. & Gai, S.L., Paper No. 13D-2, 10th Australasian Fluid Mech. Conf., Melbourne, Australia, 1989.
13. Motallebi, F. & Norbury, J.F., J. Fluid Mech., Vol. 110, p.273, 1981.
14. Liang, P. & Bershader, D., Proc. 13th Int. Symp. on Shockwaves & Shock Tubes, Niagra Falls, U.S.A., p.200, 1981.
15. Eskinazi, S., 'Vector Mechanics of Fluids & Magnetofluids', Academic Press, New York, p.175, 1967.

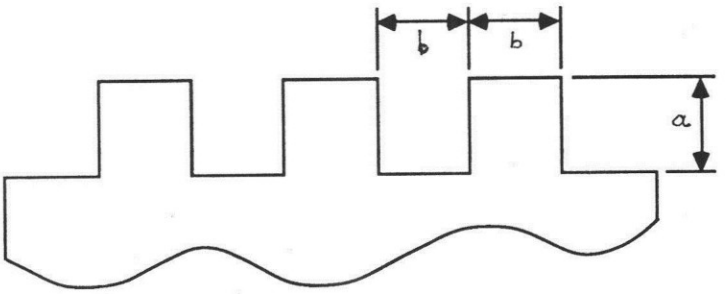

Fig. 1(a) Nomenclature for the castellations.

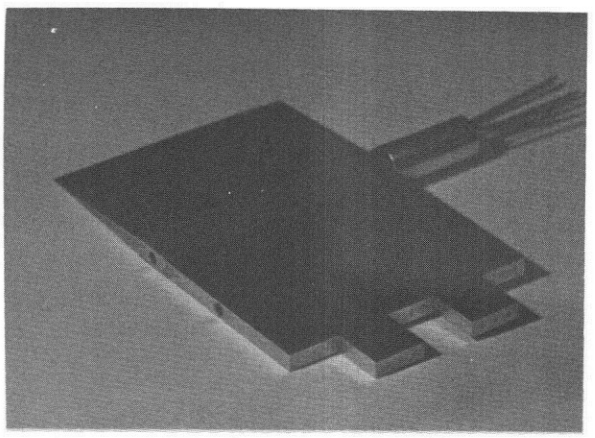

Fig. 1(b) Typical castellated blunt trailing edge model.

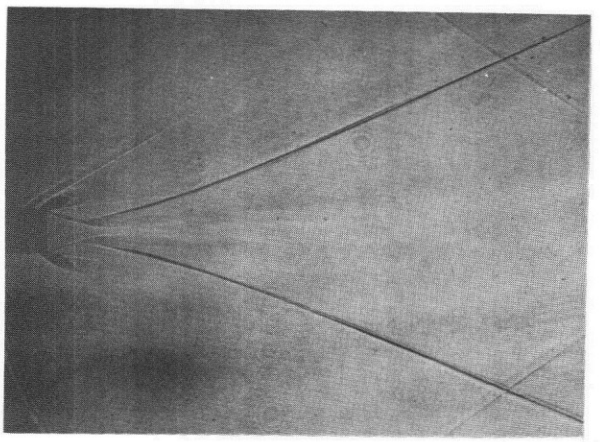

Fig. 2 Shadowgraph showing flow behind a plain blunt trailing edge model.

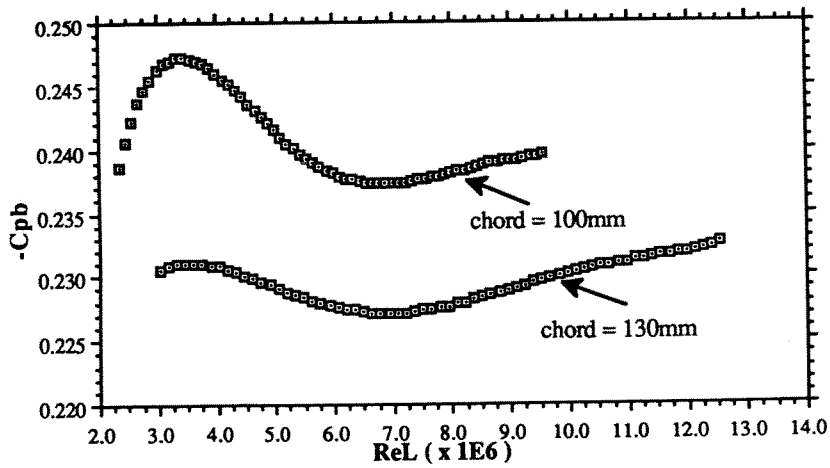

Fig. 3 Base pressure variation with Reynolds number.

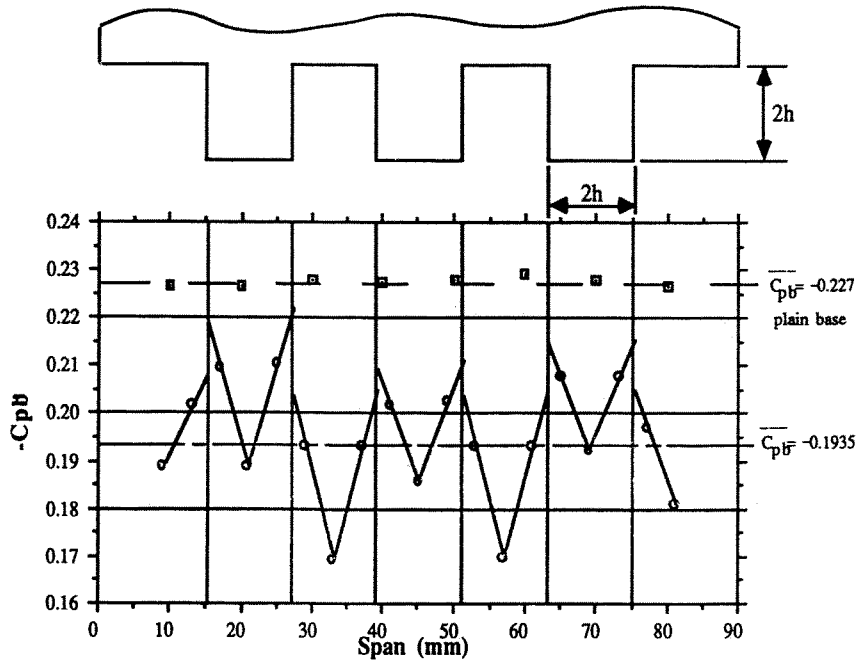

Fig. 4 Spanwise variation of base pressure for a castellated trailing edge (bxa = 12 mm x 12 mm).

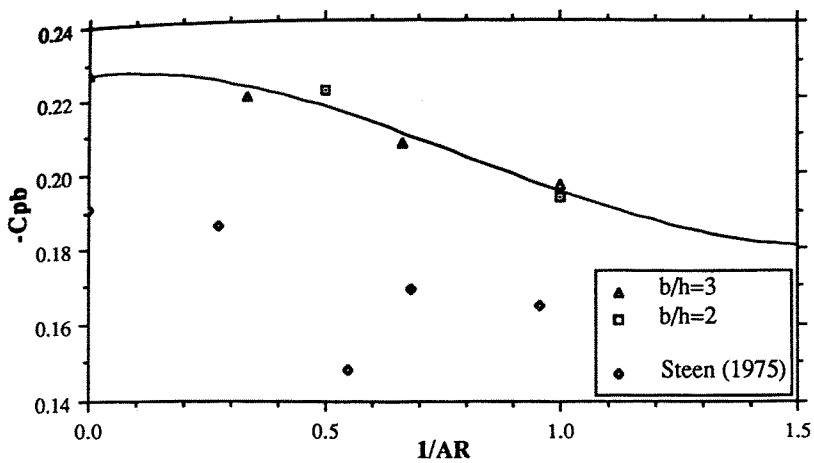

Fig. 5 Mean base pressure as a function of aspect ratio of castellations.

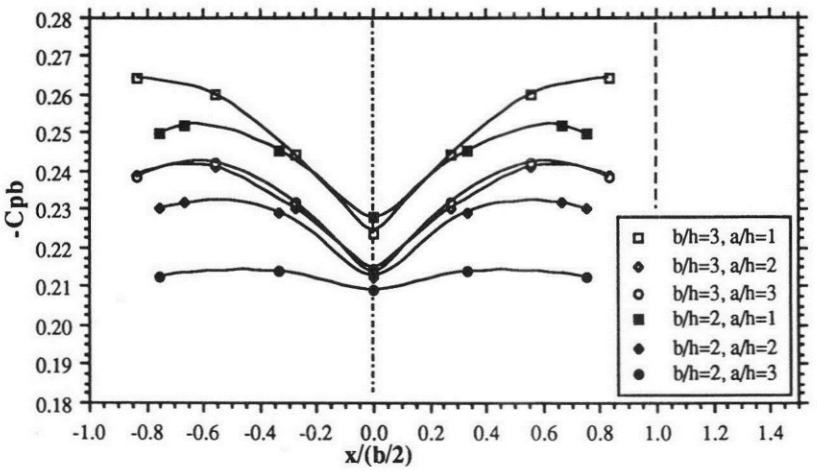

Fig. 6 Typical pressure distributions across the projection elements.

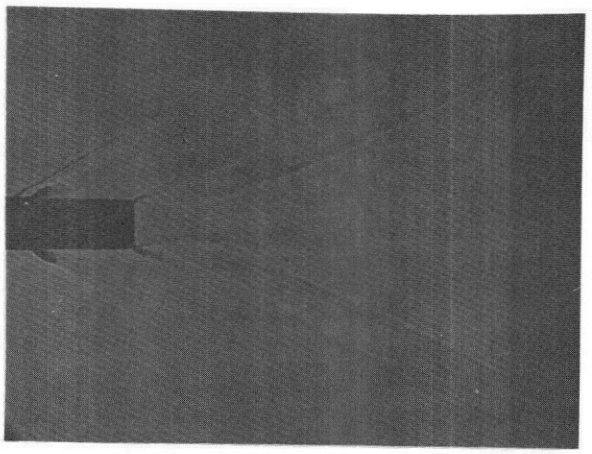

Fig. 7(a) Shadowgraph showing flow behind a castellated blunt trailing edge model (AR=1).

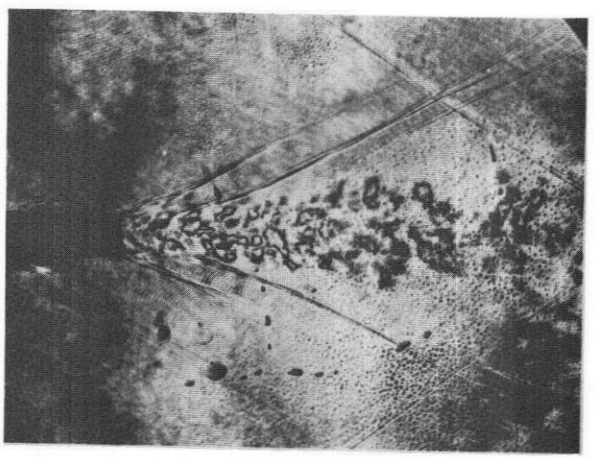

Fig. 7(b) Differential holographic interferogram of the flow behind a castellated trailing edge (AR=1).

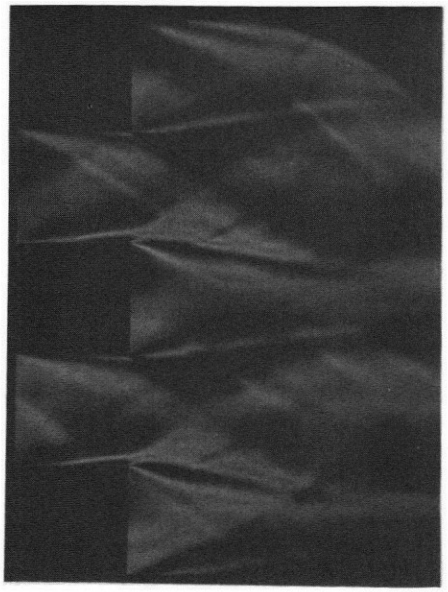

Fig. 7(c) Schlieren photograph of a castellated blunt trailing edge, looking onto span (AR=1).

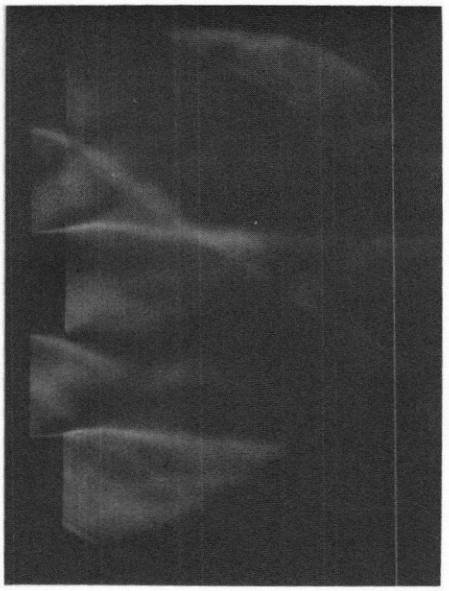

Fig. 7(d) Schlieren photograph of a castellated blunt trailing edge (AR=3).

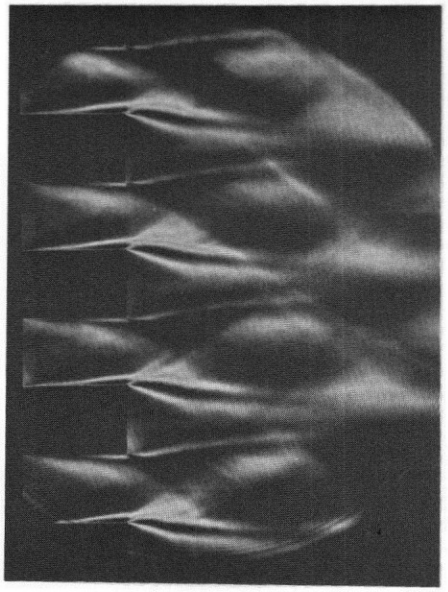

Fig. 7(e) Schlieren photograph of a castellated blunt trailing edge (AR=2/3).

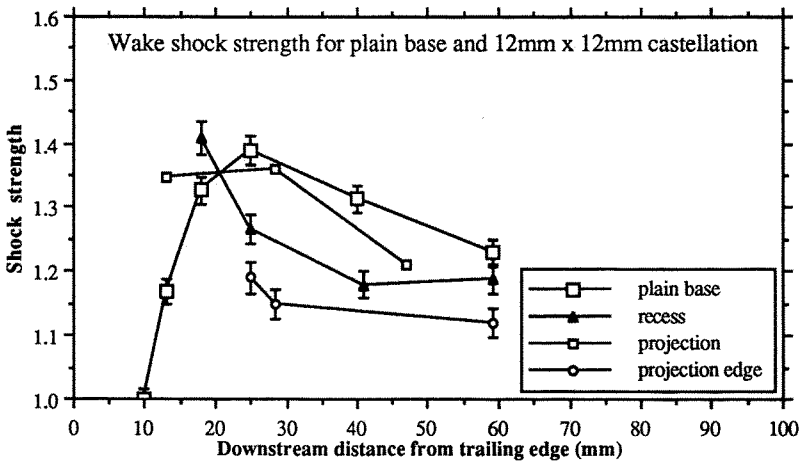

Fig. 8 Wake shock strength as a function of distance downstream from the trailing edge.

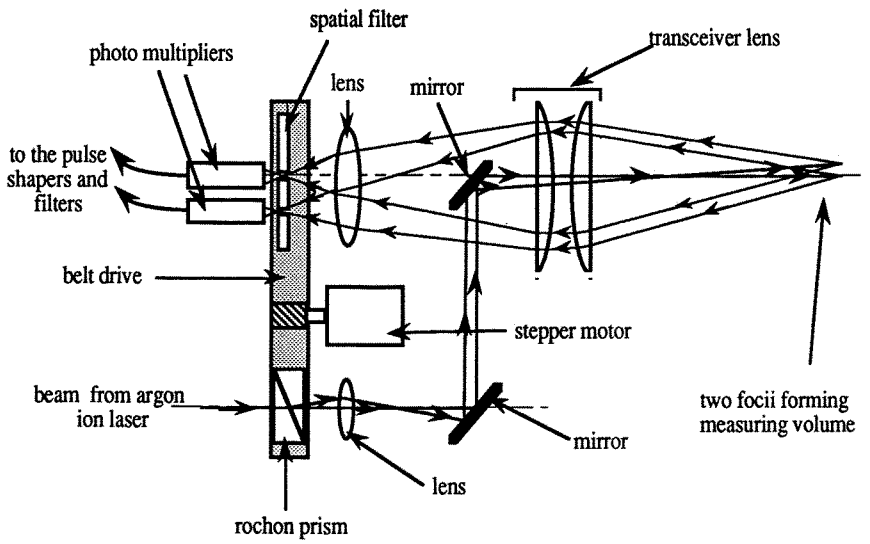

Fig. 9(a) Schematic of the optical head of the Laser 2 Focus velocimeter.

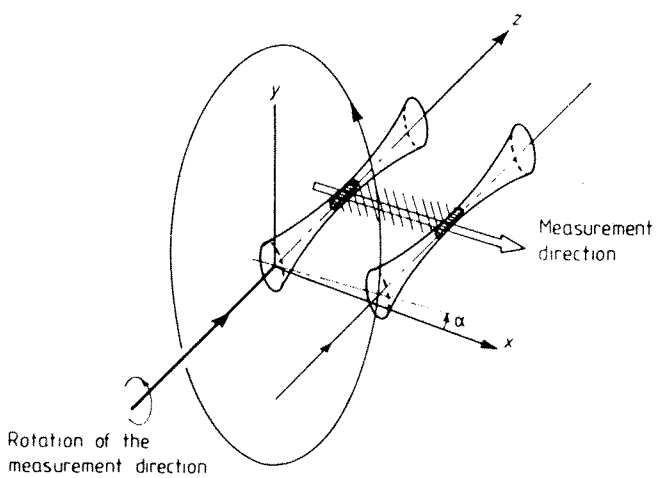

Fig. 9(b) Schematic of focal volumes and measurement direction.

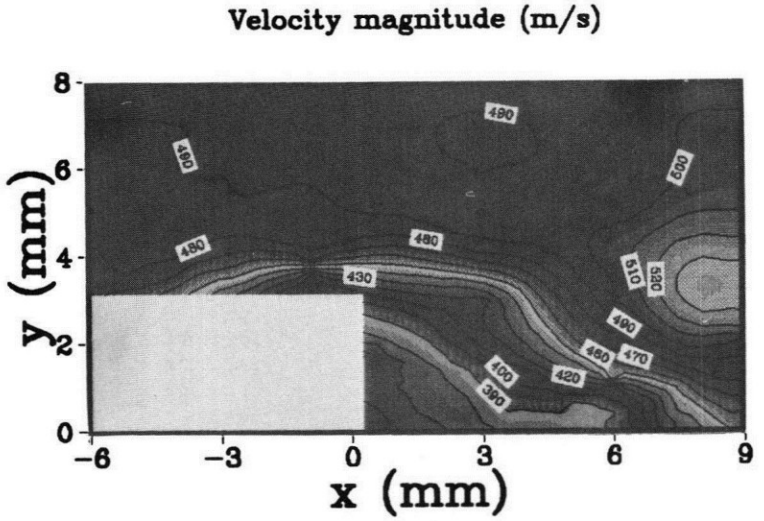

Fig. 10 Velocity contour maps.

(a) plain blunt trailing edge,

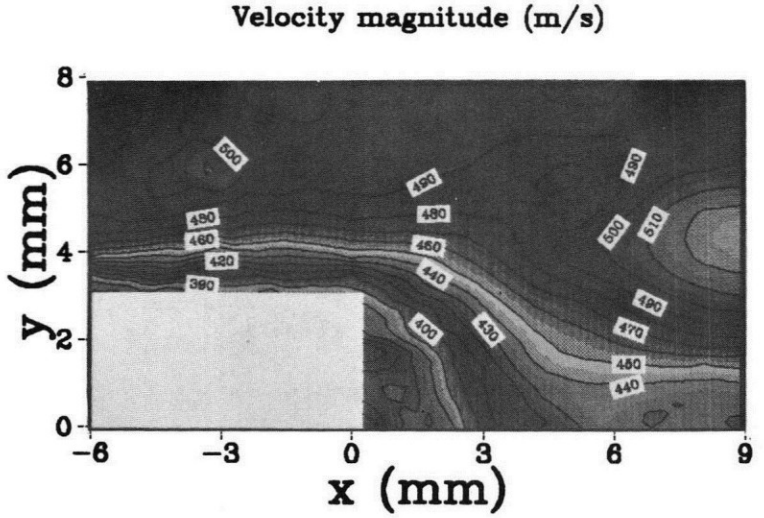

(b) centre line of the projection of a castellated trailing edge,

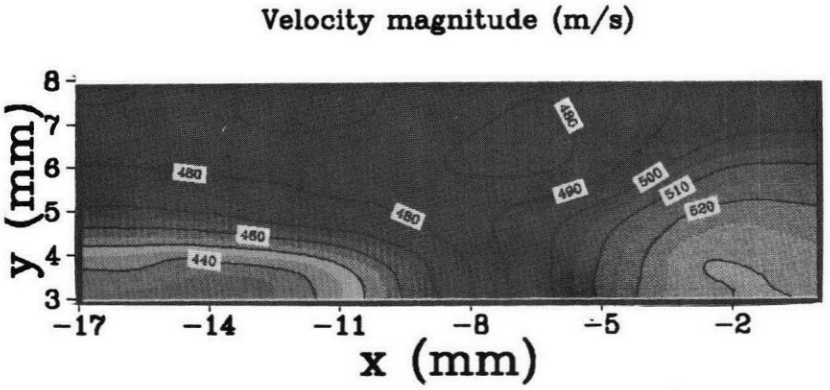

(c) centre line of the recess of a castellated trailing edge.

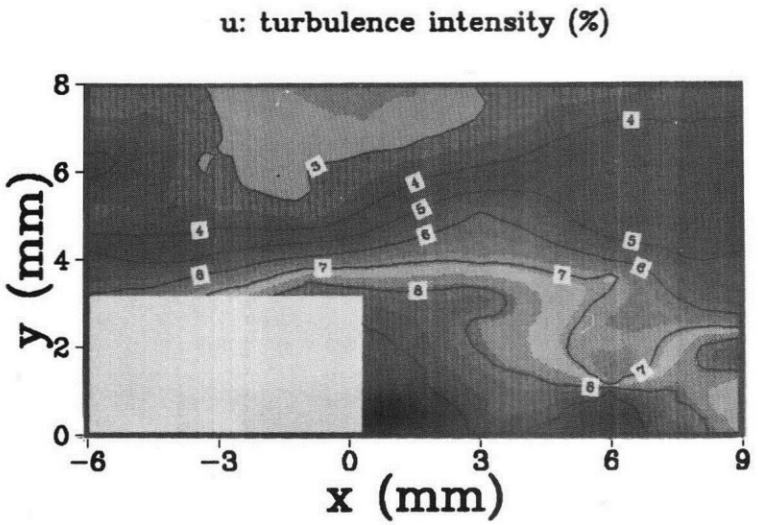

Fig. 11 Longitudinal turbulent intensity map.

(a) plain blunt trailing edge,

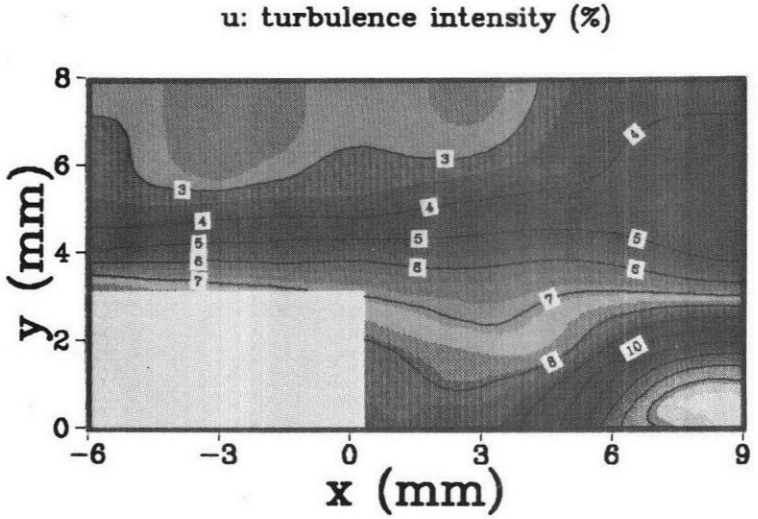

(b) centre line of the projection of a castellated trailing edge,

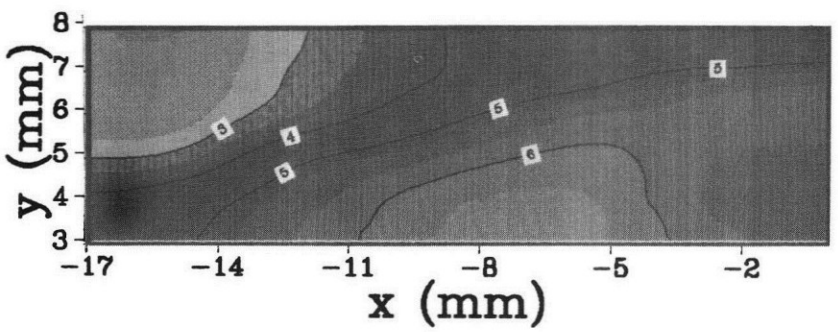

(c) centre line of the recess of a castellated trailing edge.